CHEMICAL ENGINEERING TRANSACTIONS
VOL. 91, 2022
A publication of AIDIC
The Italian Association of Chemical Engineering
Online at www.cetjournal.it
Guest Editors: Valerio Cozzani, Bruno Fabiano, Genserik Reniers

ISBN 978-88-95608-89-1; ISSN 2283-9216
DOI: 10.3303/CET2291108

Modeling of Renewable Energy Production from the Treatment of Slaughterhouse Wastewater with Ruminal Liquor in Microbial Fuel Cells

Rita J. Cabello-Torres[a]*, Esmeralda Valentin Torres[a], Lisveth Flores del Pino[b], Carlos A. Castañeda-Olivera[c], Lorgio Valdiviezo-Gonzales[d]

[a]Professional School of Environmental Engineering, Universidad César Vallejo, Campus San Juan de Lurigancho, Lima, Perú.
[b]Department of Chemistry, Universidad Nacional Agraria La Molina, Lima, Perú.
[c]Professional School of Environmental Engineering, Universidad César Vallejo, Campus Los Olivos, Lima, Perú.
[d]Universidad Tecnológica del Perú, Campus San Juan de Lurigancho, Lima, Perú.
*rcabello@ucv.edu.pe

The present study aims to optimize the application of a microbial fuel cell (MFC) in the treatment of slaughterhouse wastewater and the production of electricity. The methodology included the response surface analysis (RSA) to evaluate the effect of three factors: the standard reduction potential, SRP (copper, zinc, and graphite; electrode surface area (ESA), and the doses of ruminal liquor (DOSE). The power density (PD) and the removal of the chemical oxygen demand (COD) were determined as the main response variables. The results indicated that the generation of electrical energy depended significantly on the SRP applied, highlighting the copper-graphite arrangement that generated a maximum PD (0.5685 W/m^3) and the graphite-graphite that produced the highest removal of COD (81.33%). Consequently, the RSA produced significant predictive models for the generation of PD (R^2 = 0.9485, p = 0.029) and removal of COD (R^2 = 0.9888, p = 0.002). MFC is presented as a technology intended to be part of the diversification of renewable energy sources and at the same time recover water resources sustainably.

1. Introduction

Recently, the Intergovernmental Panel on Climate Change (IPCC) stated that to decrease the global average temperature by 1.5 to 2.0 ºC by 2050 and mitigate climate change (Li et al., 2018), renewable energy will have to cover 70 to 85% of the world's energy supply (Miller, 2020). In this context, microbial fuel cells (MFCs) applied in the treatment of wastewater used as substrate (Singh and Krishnamurthy, 2019) is a promising alternative to generate clean energy, and is a potential solution to the energy crisis (Chin et al., 2021). The efficiency of the performance of these cells is based on how well the electron is transferred from an anode to a cathode, generating electrical energy in a complete electrical circuit (Wahab et al., 2018).

MFC consists of an anode arranged in an anaerobic chamber, which contains the fuel (substrate), the biocatalyst (inoculum of cellulolytic bacteria), and an electron transport system (Dutta and Kundu, 2018). The second chamber contains a cathode catalyst and an oxidant (usually air or oxygen) (Li et al., 2018), often redox pairs are added to accelerate the reactions at the cathode. Electrons and protons are then consumed at the cathode, reducing oxygen in the form of water and generating bioelectricity (Li et al., 2018). The transfer of other unwanted chemical species is avoided by incorporating a proton exchange membrane between the anodic and cathodic chambers, which can be composed of a saturated NaCl solution combined with agar, forming a gel with chemical, mechanical, thermal stability and certain internal resistance and permeability (Dharmalingam et al., 2019; Nandy and Kundu, 2018).

Slaughterhouse wastewater has been used as a substrate and contains animal blood, hair, and other soluble organic contaminants. According to Li et al., (2018) and Kalathil et al. (2018), the process reaction can be expressed as a function of acetate decomposition, as shown in Figure 1.

Paper Received: 15 January 2022; Revised: 15 March 2022; Accepted: 22 April 2022
Please cite this article as: Cabello Torres R.J., Valentin Torres E., Flores del Pino L., Castaneda Olivera C.A., Valdiviezo-Gonzales L., 2022, Modeling of Renewable Energy Production from the Treatment of Slaughterhouse Wastewater with Ruminal Liquor in Microbial Fuel Cells, Chemical Engineering Transactions, 91, 643-648 DOI:10.3303/CET2291108

Cellulolytic bacteria from the digestive system of ruminants have also been successfully applied (Jothinathan et al., 2018), which receive electrons from the substrate and transfer them from their cell wall to the anode and then to the cathode through an external conductor generating electricity. Prabowo et al., (2016) produced significant power density (700 mW/m^2) with COD removal of less than 70% by treating slaughterhouse wastewater at 29 °C, using different doses of rumen liquor.

Lima (Peru) region has a population of more than 10 million people and a high demand for food. The slaughterhouses do not have wastewater treatment systems, and these untreated discharges end up impacting the environment. The present study aims to optimize the application of a dual-chamber microbial fuel cell (MFC) in the treatment of slaughterhouse wastewater and the production of electricity. For the modeling of the optimal operating conditions, a response surface analysis (RSA) was applied.

2. Materials and methods

2.1 Sample collections, materials, and reagents

All sample collection was performed in a slaughterhouse located in the city of Lima, using materials previously sterilized in the laboratories of the Universidad César Vallejo. Cellulolytic bacteria were obtained by applying a ruminal gold probe in the stomach of a dead ruminant. This liquid was stored in properly closed amber glass bottles. Wastewater samples were collected in plastic bottles and stored at 4ºC in a refrigerator for later use. After obtaining the sample, the experiments and analysis were carried out in the shortest possible time, due to the sensitivity of the cellulolytic bacteria.

Laboratory-scale glass MFCs were constructed using PVC tubes, copper, zinc wires, and graphite rods. Hydrochloric acid (HCl) 37% and sodium hydroxide (NaOH) granules were used in the preparation of 1M solutions to clean the electrodes (copper, graphite, and zinc rods). Potassium permanganate ($KMnO_4$) crystals and deionized water were also used to prepare an oxidizing solution(1M), arranged at the cathode for its potential as an electron acceptor to generate higher power density due to the reduction of cathodic resistance and thus increase COD removal (Ucar et al., 2017). The voltage (V) and amperage (A) measurements were performed on a Fluke D07-010771 multimeter.

The physicochemical characteristics of the substrate-inoculum mixture were determined both before and after the treatments. COD analysis was carried out using a HACH DRB200 digital reactor and a HANNA DR890 colorimeter according to the 5220 methods (APHA, 2012). The pH was measured with a HANNA HI 8424 pH meter, turbidity with a HANNA LP2000-11 turbidity meter, and ionic conductivity with a BASIC D7012292 conductivity meter.

2.3 Construction and operation of MFC

The transparent glass was used to build two MFC chambers type "H" (Figure 1) with a thickness of 5 mm, 9 cm long, 7 cm wide and 12 cm high, which were connected by a salt bridge of linear PVC tube that acted as a membrane. The chambers were sterilized with 8% formaldehyde solution. The membrane was prepared by adding 100 ml of a saturated NaCl solution (36 g NaCl/100 ml H2O) to a 10 g solution of boiling agar-agar. Before solidification of the mixture, using a syringe and from inside one of the chambers, the mixture was injected into a PVC tube (5 cm large x 1.5 cm diameter) of "H" shape inserted between the two chambers. Subsequently, the mixture was allowed to cool until it solidified forming a proton exchange membrane (PEM). An external resistor (680 Ω) was connected to the electrodes, and these were arranged as follows: a graphite electrode in the anodic chamber and a copper, zinc, or graphite electrode in the cathodic chamber. The anodic chamber was filled with the substrate (slaughterhouse wastewater) under anaerobic conditions, while the cathodic chamber was filled with 1M KMnO4 under aerobic conditions.

The current intensity of each MFC arranged in the 15 treatments was calculated based on Ohm's law: I = V/R, where I is the current intensity, V represents the voltage, and R is the resistance (680 Ω). Power, current density, and power density were also calculated as follows: P = IV; CD = I/Vol and PD =P/Vol, where P is the power, the CD is the current density, CP is the power density and Vol is the effective volume of the treated wastewater sample (0.000750 m3).

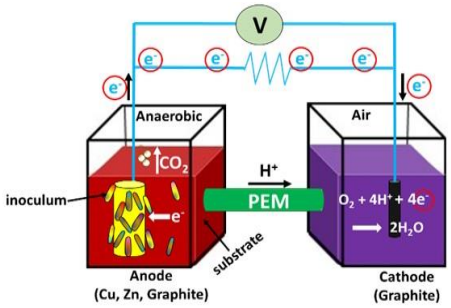

$$Anode: CH_3COOH + 2H_2O \rightarrow 2CO_2 + 8e^- + 8H^+$$
$$Cathode: 2O_2 + 8e^- + 8H^+ \rightarrow 4H_2O$$
$$Overall: CH_3COOH + 2O_2 \rightarrow 2CO_2 + 2H_2O + Biomass + Electricity$$

Figure 1: MFC chambers type "H"

The medium (substrate) was sterilized at 120 °C for 15 minutes and cooled to room temperature for the experimental execution. Subsequently, the ruminal liquor containing the cellulolytic bacteria was poured into the cell. According to the experimental design, 15 treatments were performed (in duplicate each). All treatments were carried out at 23.5°C for 7 days, without the use of nutritional salts or buffer. The electrical energy produced was measured using a Fluke D07-010771 multimeter at 6 h intervals over 7 days.

2.6 Experimental design, modeling, and statistical analysis

The Box-Behnken design was used to construct a balanced block of electrochemical tests on the graphite anode, combining 03 factors (k) such as standard reduction potential (SRP), electrode surface area (ESA) and ruminal liquor dose (DOSE), and 03 levels were established for each k factor. As k = 3, the levels were: low (-1), medium (0), and high (+1), obtaining an independent quadratic design with 15 experimental, with the following configurations: X1) Substrate/ruminal liquor ratio or DOSE: 10:0.8 (40 ml), 10:1.6 (80 ml) and 10:2.4 (120 ml); X2) ESA: 10.8; 17.6; and 24.4 cm^2 and X3) SRP: zinc (-0.76 V), graphite (0.0 V) and copper (+0.34 V). The effects of the factors (x_1, x_2, x_3) on the response variables (y) confirmed by the application of ANOVA and the prediction models for each response variable were achieved using Minitab 19 statistical software. The reliability of the results was determined using the p-value and the correlation coefficient R^2 used as decision parameters in the statistical analysis.

3. Results and discussion

The initial effluent conditions were pH: 5.6; CI: 9.05 mS/cm; turbidity: 122.4 NTU; and COD: 10,163.5 mg/L. Table 1 shows %COD, power density (PD), pH, conductivity, and turbidity values. It was observed that (considering maximum mean values) % COD: 81.83; PD: 0.57 W/m^3. The maximum PD generation was produced with the copper electrode using 17.6 cm^2 ESA and higher ruminal liquor doses (10:2.4). In de same conditions the COD removal was 71.67 %, pH: 5.96; CI: 68.3 mS/cm, and turbidity 115 NTU. The increase in CI would be due to the transport of the saturated NaCl solution present in the gel membrane (agar-agar) to the anode chamber.

Table 1. ANOVA: Significative factors on power density and COD removal from slaughterhouse wastewater

N°	X_1	X_2	X_3	% COD_{rem}	PD (W/m^3)	pH	Conductivity (mS/cm)	Turbidity (NTU)
1	0	-	-	73.69± 1.5	0.095±0.02	6.36± 0.3	50.6± 2.8	74.10± 5.2
2	0	-	+	76.16± 0.8	0.403±0.03	6.48± 0.5	50.1± 0.0	56.01±3.2
3	0	+	-	73.38±0.4	0.084±0.02	5.69± 0.1	61.7± 6.4	85.00± 8.1
4	0	+	+	76.16± 2.7	0.353±0.01	5.81± 0.7	59.6± 3.9	93.05± 5.3
5	-	0	-	73.26±1.2	0.071±0.04	5.87± 0.4	58.9± 6.4	95.04± 8.9
6	-	0	+	77.29±0.8	0.286±0.01	5.84± 0.2	66.8± 2.7	99.05±10.3
7	+	0	-	72.90± 0.3	0.104±0.02	5.82± 0.7	66.3± 3.4	103.04±10.8
8	+	0	+	71.67± 0.6	0.569±0.02	5.96± 0.4	68.3± 6.8	115.01± 1.2
9	-	-	0	**81.33± 0.5**	0.325±0.03	6.54± 0.9	73.4± 0.6	52.31± 4.1
10	-	+	0	79.47± 1.1	0.221±0.01	6.17± 0.7	56.9±3.7	41.35± 0.6
11	+	-	0	78.12± 2.9	0.350±0.02	6.48± 0.3	65.3± 4.8	64.21±5.7
12	+	+	0	77.51± 2.2	0.156±0.01	6.51± 0.1	64.2± 8.2	71.08± 4.2
13	0	0	0	79.56± 1.1	0.340±0.02	6.67± 0.3	66.7± 6.1	96.03±9.2
14	0	0	0	78.63± 1.1	0.336±0.01	6.56± 0.8	60.7± 3.9	89.12±8.2
15	0	0	0	78.94± 1.2	0.3427±0.01	6.31± 0.6	67.5± 9.1	100.08±9.9

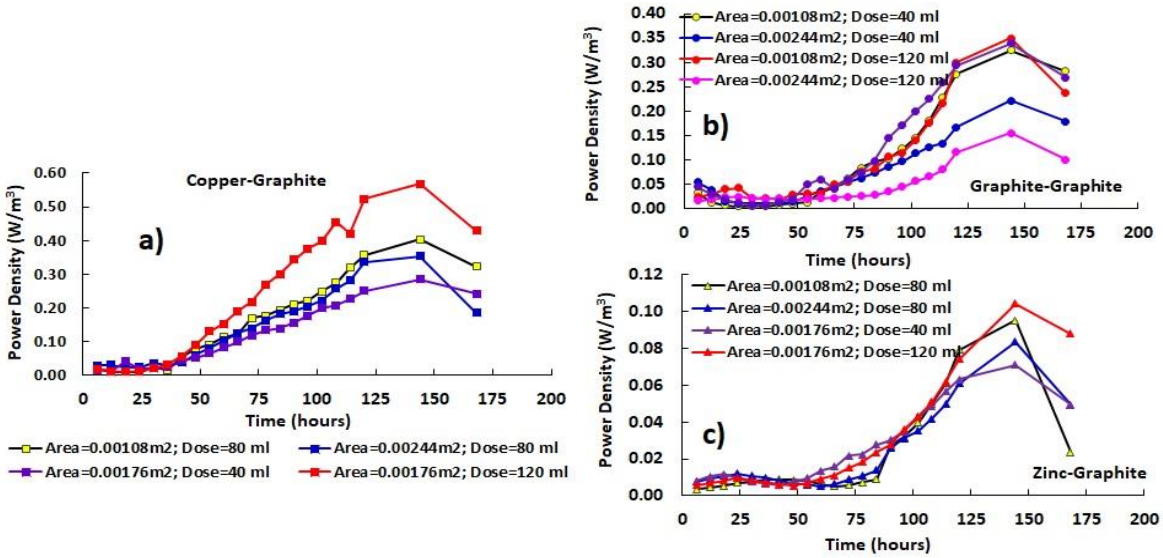

Figure 2: Temporal distribution: a) CD/Zinc-Graphite, b) PD/Zinc-Graphite and c) CD-Copper-Graphite

The effect of time on PD is present in Figure 2, it shows an increase in PD with time and its fall at 175 hours of the process, evidencing the depletion of the substrate for all electrodes configurations. In the case of the copper cathode, after the initial 25 hours of the process, there was a rapid increase in PD (0.57 W/m^3, Figure 2a), especially for an intermediate ESA (17.6 cm^2) and a higher DOSE (120 ml). A high SRP (+0.34 V) favored the process due to its higher electron-accepting capacity compared to the other materials. This advantage was previously described by Prabowo et al. (2016), for similar electrodes.

Regarding the graphite-graphite configuration, a maximum PD of 0.35 W/m^3 was achieved (Figure 2b), as Hamed et al. (2020) report. This energy generation greatly exceeded that reported by Moreno et al. (2018), who obtained values of 0.0008 W/m^3. Also, in this case, higher pH values were observed (6.2 to 6.7), this situation would imply a higher rate of proton transfer to the cathode (Prabowo et al., 2016).

Figure 2c shows less efficient results for zinc application (SRP = -0.76 V), since, after the first 50 hours, the PD increased to maximum values of 0.0950 W/m^3, in smaller ESA (10.8 cm^2). Zinc is known to have a limited lifetime disfavoring microbial growth, unlike copper which possesses a higher wear resistance (Kumari et al., 2018). In addition, Liu et al. (2020) pointed out that the biofilm could be affected by the formation of ZnO, generating stress in its structure.

Yang et al. (2018) reported that ESA from 166 to 486 cm^2 generated increasing PD values (0.2 to 0.47 mW/m^3). These contradict the values obtained, where the average PD values decreased from 0.29 to 0.203 W/m^3 as the ESA increased from 10.8 to 24.4 cm^2. This would be due to a rapid saturation of electricity production performance (Papillon et al., 2021; Shirpay, 2021).

The pH value also decreased with the increase of ESA from 10.8 to 24.4 cm^2 (see table 1 experiment 1,2,3, y 4). Several authors point out that alkaline pH generates higher power density by decreasing the production of hydronium ions due to inhibition of the more active acidogenic bacteria that dominate organic degradation (Geng et al., 2020; Sreelekshmy et al., 2020). Then, a higher area would have slowed down the electrogenic activity favoring a higher formation of organic acids. On the other hand, turbidity followed the same trend as IC, increasing its values with ESA from 10.8 to 17.6 cm^2, and then decreased with increasing ESA from 17.6 to 24.4 cm^2. Probably, changes developed in the ionization state of the functional groups (carboxyl and amino groups) present on the bacterial cell surface forming bonds with the available cations in the medium (Sreelekshmy et al., 2020); this bonding resulted in the formation of colloids increasing the turbidity.

The ANOVA results (Table 3) did not show a statistical effect on the variation of the rumen liquor dose on the response variables. However, it was observed that the higher the inoculum dose (10/0.8, 10/1.6, 10/2.4) is lower the %COD$_{rem}$. In addition, PD, and turbidity increased (see Table 1). This effect is because a lower %COD$_{rem}$ implies a higher amount of COD or substrate available in the medium, thus maintaining higher potential energy in the system (Palanisamy et al., 2019). Table 3 shows the results of the analysis of variance on the multivariable studied, such as SRP, ESA, and DOSE. The response surface analysis (RSA) applied to the data obtained generated a second-order model for the PD (W/m^3) as a function of the three factors evaluated, according to the expression (Equation 1):

$$DP = -0.014 + 0.274SRP + 0.00723DOSE + 9.6ESA - 0.148SRP * SRP - 0.000036DOSE * DOSE - 193ESA * ESA - 0.00019SRP * DOSE - 3.53SRP * ESA - 0.0562DOSE * ESA \quad (1)$$

ANOVA showed a strong correlation of the model (R^2 = 94.82%, p = 0.029), indicating that power density (PD) expressed as energy generation per fuel cell volume, is mainly affected by surface reduction potential (SRP) (p = 0.003), while ESA and DOSE did not represent a significant influence in limiting energy production (p > 0.05). This RSA analysis contradicts what was suggested by Prabowo et al. (2016) regarding the use of very dilute inoculums in substrates, which decrease electrical energy generation, since in this study the application of dilute proportions of rumen liquor (~10:1), under moderate mesophilic conditions (23.5ºC), managed to generate energy comparable to other investigations. Regarding the $\%COD_{rem}$, the following functional model was generated (Equation 2):

$$\%COD_{rem} = 85.15 - 1.23SRP - 0.365ESA - 0.0293DOSE - 15.48SRP * SRP + 0.00629ESA * ESA - 0.000141DOSE * DOSE - 0.0065SRP * ESA - 0.0353SRP * DOSE + 0.001147ESA * DOSE \quad (2)$$

Equation 2 indicated that there was a higher regression coefficient (R^2 = 98.88%, p = 0.002), with SRP and SRP*DOSE interaction being the factors that mainly affected COD removal (p < 0.05).

Figure 4 shows the 3D response surface plots for the more significant factors. Regarding $\%COD_{rem}$, Figures 4a show quadratic surfaces with higher COD removals for SRP values close to graphite (0.0 V) and in the ESA range studied (10 - 24.4 cm^2), as well as for lower inoculation volumes (DOSE: 40 ml).

The PD plots showed flat surfaces dominated by the reduction potential with maximum peaks for SRP values close to copper (+0.34 V), with relative stability for the applied ranges of ESA (Figure 4b)

Table 3. Effects of different factors on a) power density and b) COD removal from slaughterhouse wastewater.

a) Source	Adj SS	Adj MS	F-Value	P-Value
Model	118.23	13.14	23.97	0.001*
SRP	8.12	8.12	14.81	0.012*
ESA	10.18	10.18	18.58	0.008*
DOSE	0.885	0.88	1.61	0.26
SRP*SRP	66.32	66.32	121.01	0*
ESA*ESA	0.92	0.92	1.69	0.251
DOSE*DOSE	1.18	1.18	2.15	0.202
SRP*ESA	6.08	6.08	11.09	0.021*
SRP*DOSE	0.003	0.003	0	0.948
ESA*DOSE	0.389	0.392	0.71	0.438
Error	2.741	0.55		
Lack-of-Fit	2.295	0.765	3.43	0.234
Pure Error	0.446	0.22		
Total	120.98			

b) Adj SS	Adj MS	F-Value	P-Value
0.179609	0.019957	8.13	0.029*
0.093814	0.093814	38.21	0.003*
0.000116	0.000116	0.05	0.839
0.012676	0.012676	5.16	0.086
0.003897	0.003897	1.59	0.276
0.010311	0.010311	4.2	0.11
0.001177	0.001177	0.48	0.527
0.000054	0.000054	0.02	0.889
0.001617	0.001617	0.66	0.463
0.002024	0.002024	0.82	0.415
0.00982	0.002455		
0.009797	0.004899	427.06	0.002
0.000023	0.000011		
0.189429			

Significant factors: *p<0.05

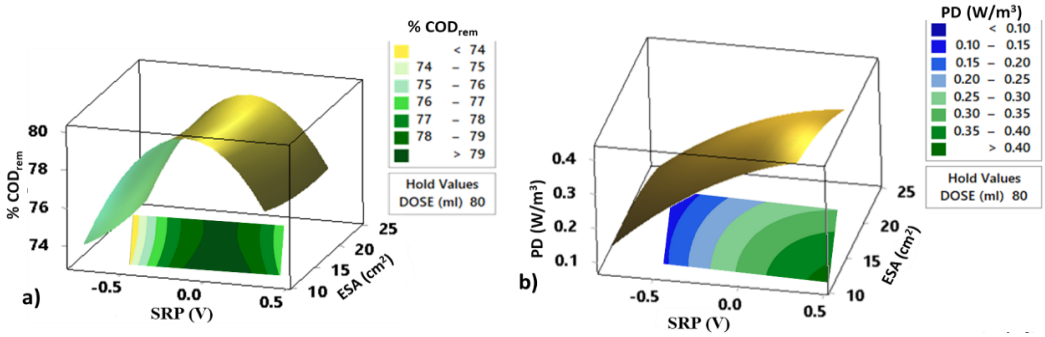

Figure 4. Three-dimensional response surface: a) $\%COD_{rem}$ vs. SRP and ESA, b) $\%COD_{rem}$ vs. DOSE and ESA

4. Conclusions

Copper electrode and a higher DOSE of ruminal liquor (80 ml) produced higher PD levels (0.57 W/m^3) for intermediate ESA (17.6 cm^2) because a larger area inhibited the activity of electrogenic bacteria, also a

significant COD removal (71.67%) was achieved. It was demonstrated that even though the wastewater had not been previously nourished with fertilizers or buffers, the energy levels produced were like those found in other investigations. Likewise, pH values close to neutrality guarantee higher efficiency in energy production and COD removal. While conductivity is an indicator that can be used to evaluate the behavior of the membrane or salt bridge configuration, turbidity was found to be a sensitive indicator to ESA. Response surface analysis produced significant quadratic models for PD generation ($R^2 = 0.948$, $p = 0.029$) and COD removal ($R^2 = 0.989$, $p = 0.002$). This method is a useful tool for predicting and monitoring new processes aimed at diversifying renewable energy sources and recovering

References

APHA (Ed) 2012, Standard Methods for the Water and Wasterwater, 19 Ed, Washington D.C, United States,

Dharmalingam, S., Kugarajah, V., & Sugumar, M., 2019, Membranes for microbial fuel cells, In Microbial Electrochemical Technology, Elsevier, 143-194.

Chin, M. Y., Phuang, Z. X., Hanafiah, M., Zhang, Z., & Woon, K. S., 2021, Exploring the Life Cycle Environmental Performance of Different Microbial Fuel Cell Configurations, Chemical Engineering Transactions, 175-180.

Dutta, K., & Kundu, P. P., 2018, Introduction to microbial fuel cells, Progress and recent trends in microbial fuel cells, 1-6.

Hamed, M. S., Majdi, H. S., & Hasan, B. O., 2020, Effect of electrode material and hydrodynamics on the produced current in double chamber microbial fuel cells, ACS omega, 5(18), 10339-10348.

Jothinathan, D., Mylsamy, P., & Benedict Bruno, L., 2018, Rumen Fluid Microbes for Bioelectricity Production: A Novel Approach, In Microbial Fuel Cell Technology for Bioelectricity Springer, Cham, 187-209.

Kalathil, S., Patil, S. A., & Pant, D., 2018, Microbial fuel cells: electrode materials, Encyclopedia of Interfacial Chemistry, 13459-13466.

Kumari, U., Shankar, R., & Mondal, P, 2018, Electrodes for Microbial Fuel Cells, Progress and Recent Trends in Microbial Fuel Cells, Chapter in: K Dutta & P Kundu (Ed.), Progress and Recent Trends in Microbial Fuel Cells, Elsevier, 125-141.

Li, M., Zhou, M., Tian, X., Tan, C., McDaniel, C. T., Hassett, D. J., & Gu, T., 2018, Microbial fuel cell (MFC) power performance improvement through enhanced microbial electrogenicity, Biotechnology advances, 36(4), 1316-1327.

Liu, C., Zhu, L., & Chen, L., 2020, Effect of salt and metal accumulation on performance of membrane distillation system and microbial community succession in membrane biofilms, Water Research, 177, 115805.

Miller, G., 2020, Beyond 100% renewable: Policy and practical pathways to 24/7 renewable energy procurement, The Electricity Journal, 33(2), 106695.

Moreno, L., Nemati, M., & Predicala, B., 2018, Biodegradation of phenol in batch and continuous flow microbial fuel cells with rod and granular graphite electrodes, Environmental technology, 39(2), 144-156.

Papillon, J., Ondel, O., & Maire, É., 2021, Scale-up of single-chamber microbial fuel cells with stainless steel 3D anode: Effect of electrode surface areas and electrode spacing, Bioresource Technology Reports, 13, 100632.

Palanisamy, G., Jung, H. Y., Sadhasivam, T., Kurkuri, M. D., Kim, S. C., & Roh, S. H., 2019, A comprehensive review on microbial fuel cell technologies: Processes, utilization, and advanced developments in electrodes and membranes. Journal of cleaner production, 221, 598-621.

Prabowo, A. K., Tiarasukma, A. P., Christwardana, M., & Ariyanti, D., 2016, Microbial Fuel Cells for Simultaneous Electricity Generation and Organic Degradation from Slaughterhouse Wastewater, International Journal of Renewable Energy Development, 5(2).

Shirpay, A., 2021, Effects of electrode size on the power generation of the microbial fuel cell by Saccharomyces cerevisiae, Ionics, 27(9), 3967-3973.

Sreelekshmy, B. R., Basheer, R., Sivaraman, S., Vasudevan, V., Elias, L., & Shibli, S. M. A., 2020, Sustainable electric power generation from live anaerobic digestion of sugar industry effluents using microbial fuel cells, Journal of Materials Chemistry A, 8(12), 6041-6056.

Ucar, D., Zhang, Y., & Angelidaki, I, 2017, An overview of electron acceptors in microbial fuel cells, Frontiers in microbiology, 8, 643.

Wahab, K. A. A., Nazri, A. A. A., Azam, A. A. M., Ghazali, N. F., Salleh, E. M., & Mahmood, N. A. N., 2018, Development of immobilised bioanode for microbial fuel cell. Chemical Engineering Transactions, 607-612.

Yang, Y., Yan, L., Song, J., & Xu, M., 2018, Optimizing the electrode surface area of sediment microbial fuel cells. RSC advances, 8(45), 25319-25324.